Journal of the European Ceramic Society 43 (2023) 5148–5158

Contents lists available at ScienceDirect

Journal of the European Ceramic Society

journal homepage: www.elsevier.com/locate/jeurceramsoc

Three-dimensional preforming via wet-laid nonwoven technology for ceramic matrix composites

Fiona Kessel [a,*], Martin Frieß [a], Oliver Hohn [b], Linda Klopsch [a], Charlotte Zöllner [a], Cora Dirks [a], Matthias Scheiffele [a], Felix Vogel [a], Raouf Jemmali [a]

[a] Institute of Structure and Design, German Aerospace Center e.V., Stuttgart, Germany
[b] Institute of Aerodynamics and Flow Technology, German Aerospace Center e.V., Cologne, Germany

ARTICLE INFO

Keywords:
3D Preforming
Ceramic matrix composites (CMC)
Wet-laid nonwoven
Wind tunnel test
Liquid silicon infiltration (LSI)

ABSTRACT

In this study, a new 3D preforming method was developed using wet-laid nonwoven technology, for application in manufacturing ceramic matrix composites (CMC). For this purpose, a process setup was developed and tested on an example geometry (radome). HTS 45 carbon fibers and Nextel610 alumina fibers were used for the preforming. The resulting C/C-SiC and OXIPOL materials were mechanically characterized and the microstructure was investigated. A radome was manufactured from each material and subjected to DLR's L2K and VMK wind tunnels. The tests have been successful with the C/C-SiC and OXIPOL radome. Overall the application-oriented tests show that load-bearing components can be produced with the newly developed preform method and that they also prove themselves in the application. The knowledge gained, demonstrates the potential of the 3D wet-laid nonwoven preforming method and represents a new possibility for CMC production with complex shapes.

1. Introduction

Fiber-reinforced composites are a worldwide used group of materials for applications that demand fracture toughness and high temperature stability. While it is relatively simple to vary the reinforcing fiber types or switch to different matrix systems it remains difficult to realize complex preforms which follow the component shape [1–3]. In most cases the fiber reinforcement is aimed to enhance the mechanical stability and toughness of the component by following its outlines. In addition, the need for an accurate preform increases dramatically when using expensive raw material, since waste from the manufacturing needs to be reduced to a minimum for economic and ecological reasons [4]. For ceramic matrix composites (CMC) those criteria are especially true, since the material is very costly and used in some of the most challenging environments. These environments demand superior material properties (e.g. carbon fiber reinforced silicon carbide (C/C-SiC) for rocket nozzles, silicon carbide fiber reinforced silicon carbide (SiC/SiC) turbine shrouds for jet engines) [5–7]. The group of radomes is one such component category where CMCs are a favorable material due to its excellent performance. However, accurate preforming is quite difficult to realize for the complex shape of those structures. For flight stability and reduced air friction, the tip geometry is best designed pointed, leading ogive-shaped to the main body. However, this geometry causes high temperatures at the very tip that range from 900 °C to 2000 °C depending on the trajectory [6]. The creation of such ogive-shaped preforms suitable for radome structures is a daunting challenge and the available textile technologies often come with downsides for the structure.

Frieß et al. demonstrated the creation of a ogive-shaped radar transparent radomes with different preforming methods and highlighted some of the difficulties in their manufacturing [8]. One radome was made of several layers of woven fabric, whereby the single layers where tailored to achieve the desired shape. In consequence the fabrics were cut to be draped and had multiple cutting edges in every single preform layer, leading to an interrupted reinforcement. With the woven preform style manual draping was involved and cutting waste could not be avoided. The second method was filament winding. While the base shape of the radome could be produced, the very tip remained difficult. The filaments slipped on the small radius and limited therefore the shaping possibilities. These difficulties were counteracted by placing two radome-shaped winding body's opposite each other and connecting them with a small bar, which allowed a non-slipping winding process. However, the tip needed to be replaced and was manufactured separately by routing it out of a plate of thick CMC material. Later, the two components were joined to obtain the final product [8].

* Corresponding author.
E-mail address: fiona.kessel@dlr.de (F. Kessel).

https://doi.org/10.1016/j.jeurceramsoc.2023.04.062
Received 6 December 2022; Received in revised form 24 April 2023; Accepted 28 April 2023
Available online 29 April 2023

Another interesting technology for cone like preforms was described by Chen at al. which focuses on nonwoven preforms via three-dimensional needle-punching. They described the newest possibilities of the needle-punching technology as well as microstructure and mechanical properties of C/SiC material [9,10]. Via winding of small nonwoven tapes on a cone-shaped core a three dimensional preform was obtained. During the winding process the tapes were needle-punched and thus the overlapping tapes consolidated. This process evolved in to robotic assisted needle punching, whereby a single or very few needles are placed on a robotic arm with five axes. The arm is then capable to consolidate a fiber fleece on a stitching core with the shape of the desired 3D preform. Still so far, no cone shaped, 3D needle-punched CMC was manufactured. One possible explanation could be the generally lower compressibility of needled nonwovens compared to e.g. woven fabrics caused by fibers oriented in the direction of the compression force (z-direction) [11,12]. The result is a lower fiber volume fraction (FVF) in the nonwoven and a CMC with low fracture toughness.

Regarding new methods with potential for three-dimensional preforming, a type of nonwovens was investigated in previous work which offer such possibilities. It is the sub-group of wet-laid nonwoven which offer a wide range of shaping possibilities due to its unique manufacturing process and the resulting textile has very few fibers in thickness direction which allows a higher FVF than regular nonwovens. It was found, that depending on the fiber preparation during the fabric manufacturing, short fiber reinforced ceramics as well as monolithic ceramics are obtainable [13]. The manufacturing of the wet-laid nonwoven ceramics is summarized in Fig. 1 and shows their two possible microstructures. During the former studies, an interesting possibility was found for manufacturing not only flat nonwoven fabrics, but as well to manufacture three dimensional preforms. Originally the process derived from the paper-manufacturing technology. Here the process consists of dispersing a cellulose fiber mass in water which is dewatered over a screen resulting in paper or likewise in a wet- laid nonwoven fabric, (analog to the scheme in Fig. 1). The same process is applied to receive three dimensional shaped papers or cartonnage. The commonly best-known example for a product based on this process are egg trays as well as other tailored product packaging [14]. These carton packaging have astonishing features like a very versatile shape with small radii and steep angles between neighboring areas, features that are desired for textile preforms targeting complex composite components. In addition, the manufacturing process is very flexible, and can be adapted to different component shapes and can be produced in large quantities in a short time [15].

Aiming at the three-dimensional preforming of fibers, the experience of the previous work with wet-laid nonwovens was combined with the technology of the cartonnage shaping to develop such a process. The technology was developed to target as an example the shape of radome structures and to evaluate its potential for crucial parts like the tip and steep angles. A simple laboratory set up was designed to manufacture the preforms. However, due to the novelty of the 3D-process fundamentals regarding control over fiber behavior were assessed as well. This includes the creation of a C/C-SiC flat sample and a radome for characterization, followed by a transition to Nextel 610 alumina fibers (3 M), which are of interest due to its radar transparency. The C/C-SiC components were manufactured via the liquid silicon infiltration (LSI-process) whereas the Nextel 610 preform was processed via polymer infiltration and pyrolysis (PIP-process) to yield a ceramic material called OXIPOL. The alumina fiber demonstrator was tested in the two wind tunnels at DLR Cologne (*Arc-heated wind tunnel 2* (L2K) and *Vertical test section Cologne* (VMK)) to evaluate the material for the radome application. The tests showed the impact on the wet-laid nonwoven based radomes and their load-bearing capacity. For further insights computed tomography was used to monitor defects and changes in the structures.

2. Material and methods

2.1. Design of the 3D wet-laid nonwoven process

In order to implement the idea of producing wet-laid nonwovens in a 3D process, a laboratory setup was designed with which the textile preforms could be realized (see Fig. 2a). This consists of a container for a fiber/water suspension, a connected pump circuit and a positive mold (core) for the 3D textile. The vessel is designed in such a way that

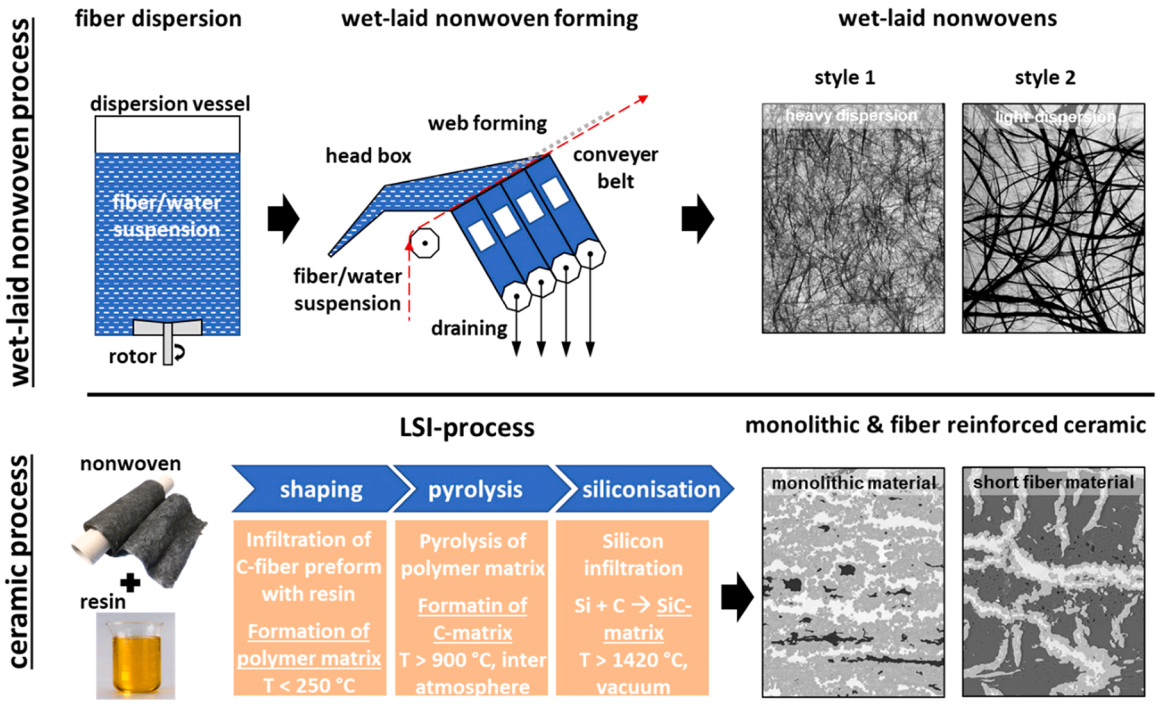

Fig. 1. Upper part: Scheme of the wet-laid nonwoven process and possible nonwoven styles, lower part: Scheme of LSI-process and the microstructure of the resulting ceramics based on the two wet- laid nonwoven styles [13].

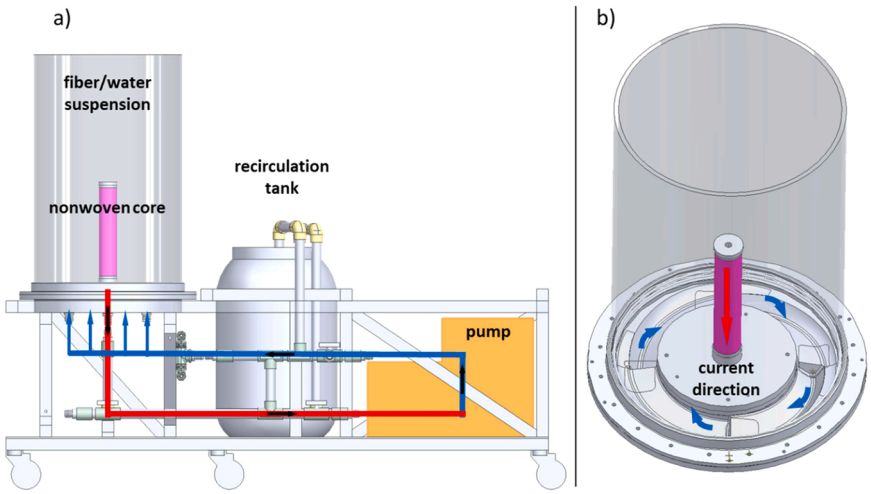

Fig. 2. a) 3D-wet-laid nonwoven device for the manufacturing of three dimensional preforms, b) suspension tank with indication of the direction of the current.

different cores can be installed and thus the preforms are variable. For the production of the preforms, the water pumping is activated and the suspension flows to the core. In the initial setup, the water flow was designed to form a vortex due to the radial inflow, which is intended to prevent the fibers from sedimenting and to continuously flow fibers past the core (see Fig. 2b). The core was initially irregularly covered with fibers, since the suction effect is higher the closer the core openings are to the suction point. Homogenization of the preform only occurs in the course of the manufacturing process, when core openings that are already covered by fibers, shift the suction to less covered areas thus experience a higher suction (see Fig. 3).

The wet-laid nonwoven system is operated with the pump AL-KO Jet 6000/5 premium from the AL-KO Geraete GmbH with a flow rate of 6 m^3 /h. The fiber/water suspension is set to 60 liters and a fiber concentration of 0.17 g/l. To keep this constant, 10 g of fibers (carbon fibers) are added to the process water every two minutes since the fibers are mostly settled on the core after that time (respectively 20 g alumina fibers because of their higher density of the fibers). To consolidate the preforms, carboxymethyl cellulose is added as a binder, which stabilizes

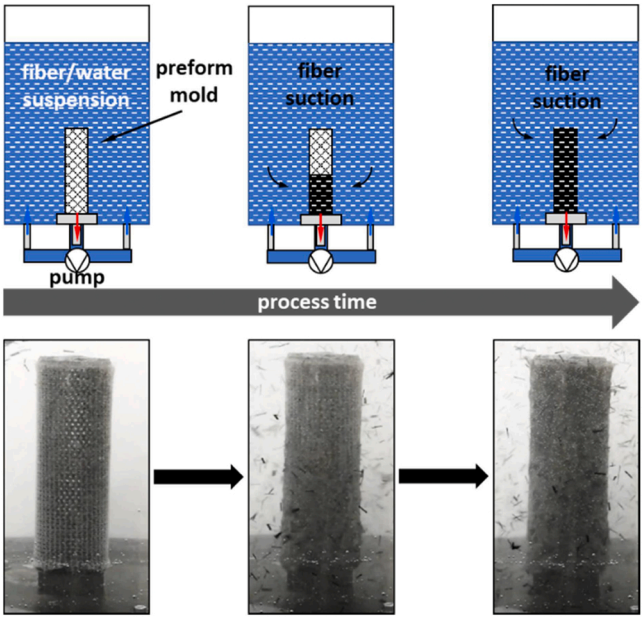

Fig. 3. Formation and fiber buildup of the 3D preform in the wet-laid nonwoven process.

the preform. The fiber addition is repeated until no more fibers appear to be deposited on the core. The water recirculation is then stopped and fed into the recirculation tank. This causes the water container to run dry and the preform to be exposed. The core with the preform can then be removed and dried. In this work, two different core structures were used: a cylindrical one, which yields a textile surface for sheet material, when cut open and removed from the preform. These sheets have been used for ceramic characterization. As the second geometry, a radome tip, was designed to produce the CMC component for wind tunnel testing. This geometry was used to verify how well complex designs can be implemented using the wet-laid technology. All relevant manufacturing conditions are summarized in Table 1.

2.2. Raw materials

According to the experimental procedure shown in Fig. 4, two fiber materials were investigated in the 3D wet laid nonwoven process: HTS45 carbon fibers (C-fiber, with epoxide sizing) from Toho Tenax Europe GmbH and Nextel 610 alumina fibers (Al_2O_3-fibers, with PVA sizing) from 3 M Deutschland GmbH. The C-fibers were used for technology testing and for the production of C/C-SiC sheets, analogous to the two-dimensional wet-laid C/C-SiC from previous work [13]. In addition, a radome was fabricated from C/C-SiC. Nextel 610 fibers were used to fabricate OXIPOL (oxidic CMC based on polymers) ceramics. The ceramic fiber enables the production of fiber-reinforced ceramic materials that are not electrically conductive and thus radar transparent which is required for radomes.

As an important step to make the fibers processable in the 3D preform process, a sizing has to be applied. Previous work has shown how important the preservation of the fiber bundles is for achieving fiber reinforcement and an acceptable fiber volume fraction [13]. Up to now, attempts have been made to preserve the fiber bundle structure exclusively by reducing mechanical action during the wet-laid nonwoven process. Since the force can only be adjusted or reduced to a limited extent within the laboratory set-up, the following investigations focused on fiber bundle retention via fiber sizing. Polyvinyl alcohol (PVA) was selected as the fiber sizing (PVA, ThermoFisher Scientific). PVA has very

Table 1
Process parameters for the 3D wet-laid nonwoven process.

Parameter	Values
pump volume flow	6 m^3 /h
binder concentration	0.03 g/l
fiber concentration	0.17 g/l
process time	10–20 min

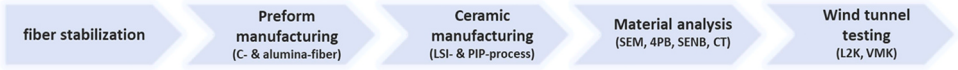

Fig. 4. Experimental proceeding for the creation of the radome tip for wind tunnel testing.

good adhesive properties and exhibits solubility in water depending on the degree of hydrolysis. Thus, it allows the preparation of a simple water-based coating [16,17]. However, crucial for its suitability is that thermal aging can increase the degree of crystallization of PVA, thus worsening its water solubility again [18]. Based on these properties, it was possible to design a coating concept in which the fibers are first coated with a self-produced sizing and then it is rendered water insoluble by thermal aging. This prevents the bonded fiber bundles from dissolving in the wet-laid process.

According to the experimental proceeding in Fig. 4, the influence of the sizing was first investigated (as received, sized, sized + thermal treatment). For this purpose, accordingly prepared fibers were dispersed in demineralized water (200 rpm) for 5 min, at a fiber/water concentration of 0.167%. Frames of the dissolution process at 10 s (start) and 300 s (end). Allow qualitative comparison of fiber bundle dissolution.

This basic study to preserve the fiber structure is followed by the production of the nonwovens for the mechanical characterization, microstructure analysis and for the wind tunnel tests. This is done accordingly as described in the section on the design of the 3D wet-laid nonwoven process. For the production of the CMC plates and radome components, different matrix systems are used depending on the process. For the C/C-SiC samples produced in the LSI process, a carbon precursor is mandatory as the matrix. A phenolic resin from Hexion Group is used for this purpose. For the OXIPOL ceramics, a polysiloxane from Merck KGaA is used. The material is produced via the PIP process and the component is infiltrated several times with the polymer.

2.3. Ceramic manufacturing via LSI-process

The C/C-SiC ceramics are manufactured using the LSI process as shown in Fig. 1. It includes three process steps: First, the ceramic green body fabrication. This involves the production of a CFRP body, which is created by infiltrating, or impregnating, a preform in a mold with resin and then curing it. For all specimens and components, resin transfer molding (RTM) was used as the molding method. Second, the pyrolysis of the green body. In this process, the green body is heated to over 900 °C in an inert gas atmosphere and the phenolic matrix decomposes to an amorphous carbon matrix and a crack structure forms in the C/C body. The third and last step is the siliconization: Here, in a second high-temperature step under vacuum, silicon granulate is melted at temperatures above 1420 °C. It then infiltrates into the porous C/C body, where the liquid silicon reacts with the amorphous carbon in the pore interfaces to form silicon carbide [19,20].

2.4. Ceramic manufacturing via PIP-process

For the production of the OXIPOL ceramic, the PIP process is used [6,8]. For the manufacturing of the ceramic green body a polysiloxane matrix as precursor is infiltrated via RTM. After shaping, an initial pyrolysis is conducted above 1300 °C in inert gas atmosphere. Analogous to the LSI process, a porous matrix is formed, in composition already corresponding to the final SiCO ceramic matrix. However, the porosity is too high (approx. 30–40%) after only one infiltration and pyrolysis cycle. In order to create a sufficient bond between fiber and matrix and thus improve the structural mechanical properties, the steps of polymer infiltration and subsequent pyrolysis are repeated several times. This densifies the matrix and completes the ceramic manufacturing process [21]. Four cycles were performed for the fabrication of the OXIPOL plate and six cycles for the radome.

2.5. Characterization

During material production, the density and porosity of the samples were determined in all process steps. The Archimedes method according to DIN EN 993 − 1:1995 − 04 was used for this purpose. For the production of the OXIPOL radomes, the number of cycles required to achieve a target porosity of less than 10% was determined. In order to investigate the manufacturing results of the ceramics, the microstructure of all of them was examined. The Gemeni Ultra Plus scanning electron microscope (SEM) from Zeiss GmbH was used for this purpose with an AsB (Angle selective Backscattered electron) detector. Based on the images, the phase composition was determined using the open source software ImageJ (Version ImageJ 1.52p, Java 1.8.0_172 (64-bit)) via a gray value distribution.

To test the mechanical strength of the materials, samples (n = 5) were taken from each of the sheet materials for four-point bending tests according to DIN-EN 658 − 3:2002 − 11. The samples were cut with a diamond blade equipped circular saw in the dimensions of 10 mm × 100 mm × 3 mm to have an L/D ratio of 20 for the test setup. A universal testing machine (Zwick 1494) was used to perform the test with a controlled cross head speed of 1 mm/min. Samples were tested to failure and the mean and standard deviation of the test results were determined. The fracture toughness was investigated using single edge notched bend testing (SENB) as proposed by Kuntz et al. [22]. Therefore, a three-point bending test is performed on a pre-notched specimen, on a Zwick 1494 with a controlled cross head speed of 1 mm/min. The samples were prepared using abrasive cutting with a saw blade of 300 μm thickness (4.0 mm × 5.0 mm × 22.5 mm, pre-notch 2.0 mm)). In addition, the interlaminar shear strength (ILSS) was tested according to DIN EN 658–4: 2003. For this purpose, double-notched specimens (n = 5) were loaded under pressure. For specimen preparation, appropriate material was ground flat (specimen thickness 3 mm) and then specimens were machined out using abrasive cutting (25 mm × 10 mm). The two large specimen sides were notched with a penetration depth of 1.5 mm (half specimen thickness). The notches are staggered so that there is a notch distance of 8 mm in the center of the specimen and the specimen fails interlaminar in this area. The tests were also performed with a Zwick 1494 and a controlled cross head speed of 1 mm/min.

In order to assess the uniformity of the textile preforms, the radomes were examined after fabrication using computed tomography. The measurements were conducted using a high-resolution μCT-System (v|tome|x L, GE Sensing & Inspection Technologies GmbH, Wunstorf) consisting of a microfocus X-ray tube with a maximum accelerating voltage of 240 kV and a 16-bit flat panel detector (active area 2048 × 2048 pixels at 200 μm per pixel). The μCT scans were performed with the X-ray parameters 200 kV/750 μA at an exposure time of 267 ms. A voxel size of 170 μm could be achieved. The μCT data were visualized and analyzed with the commercial software package VGStu-dioMax 3.4 (Volume Graphics, Heidelberg). To investigate the influence of the wind tunnel test, the radomes were scanned again after the testing.

2.6. Wind tunnel testing

For the qualification of the materials, tests in two different wind tunnels were conducted with radomes. The Vertical Test Section (VMK) and the arc-heated wind tunnel L2K of DLR Cologne were used for this analogous to previous qualification testing of high speed missile radomes [6]. The facilities are described in detail by Triesch and Krohn [23] (VMK) and Gülhan et al. [24,25]. A combined approach with testing

in two facilities is necessary to fully validate the radomes, as it is not possible to directly replicate the flight conditions of the envisaged missions with flight Mach numbers above Ma = 4 and correspondingly high heat and mechanical loads in only one facility. Though falling short the real flight conditions, tests in VMK, which can achieve direct flight conditions up to Mach 3 in an altitude of 4.5 km, give valuable information as the radome is subject to both high aerothermal and mechanical loads as well as thermal shock. In L2K, on the other hand, flight relevant heat loads can be imposed on the radome that correspond to those a radome missile would experience during its planned mission. Here, however, the density and pressure, and consequently the Reynolds number, are very low and the aeromechanical loads are accordingly smaller. The flow conditions of the tests in in L2K and VMK are listed in Table 2 and Table 3, respectively. In L2K, three different conditions were tested to simulate cases with a moderate heat flux and longer test duration, resulting in a high integral heat load (condition FC1), and two conditions with high and maximum heat fluxes but short test durations, and thus lower integral heat load but higher heat fluxes (and potentially wall temperatures) in the stagnation region of the radome. In addition to this, the angle of attack was varied ($\alpha = \pm 10°$ in L2K and $\pm 5°$ in VMK), also in combination with different roll angles (0° and 90°, to determine the impact of different flight angles on the thermal behaviour and, more importantly, an additional bending moment from the aerodynamic forces in VMK testing. By variation of angle of attack and roll angle, the direction of the thermal and mechanical loads is changed as well. In both VMK- and L2K-testing, the temperature distribution on the external surfaces was measured by infrared thermography and on the internal wall by thermocouples. The experimental setup is the same as the one described in [6].

3. Results

3.1. Fiber stabilization

3.1.1. Carbon-fiber

The first tests were aimed at stabilizing the fiber bundles. As discussed previously, the goal is to avoid fiber bundle dissolution as much as possible in order to produce a damage tolerant short fiber material. To investigate the effect of fiber sizing on fiber dissolution, the fibers were tested 'as received', 'sized (2% PVA)' and 'sized (2% PVA) + tempered' in a laboratory test. The qualitative comparison of the dissolution tests is shown in Fig. 5a) and shows the dissolution process at the beginning of the process (10 s) and at the end of the process (after 5 min). Despite identical fiber consistencies, a direct difference in the fiber dissolution can already be observed in the first 10 s. The newly *sized* fibers tend to separate directly at the beginning of the exposure process. By the end of the process, this effect increases significantly and the fibers are present as fanned-out fiber flocks without a bundle structure. In the case of fibers in the *as received* state, the bundle structure persists longer, and even towards the end of mixing, isolated intact fiber bundles are still present. Nevertheless, their further disintegration is likely with stronger dispersion power, or longer running process times, as was also seen in unpublished data. The smallest change in the bundle structure was observed in the newly sized fibers with subsequent tempering. Here, the bundle structure remains largely intact, even over the entire dispersion time. Based on these results, fiber preparation in the form of sizing and subsequent tempering was selected for the production of 3D wet-laid nonwovens.

Table 2
L2K test conditions.

Test condition	L2K-1	L2K-2	L2K-3
mass flow [g/s]	110	110	110
hot/cold gas ratio [g/s]	50/60	60/50	65/45
reservoir pressure [hPa]	2000	2360	2570
total enthalpy [MJ/kg]	2,6	3,8	4,8
reservoir temperature [K]	2193	2905	3304
Pitot pressure [hPa]	89	136	597
heat flux [kW/m2]	945	1810	2725
test duration [s]	80	6	6

Table 3
VMK test conditions.

Test condition	VMK
Mach number	3
total pressure p_{t0} [MPa]	2.1
total temperature Tt0 [K]	700
unit Reynolds number $Re_{m\infty}$ [10^6/m]	47.4
test duration [s]	30

3.1.2. Alumina-fiber

According to the manufacturer 3 M, the alumina fiber is already sized with PVA. However, as shown in the experiment, the fibers dissolve very quickly into individual filaments on contact with water (see Fig. 5b)). To prevent this, the *as received* fibers were tempered as well. The results show that, analogous to the carbon fibers, the thermal treatment has a sizing stabilizing effect. Therefore, all alumina fibers were thermal stabilized before the 3D wet-laid nonwoven process.

3.2. 3D wet-laid nonwoven process

The first preforms produced using the new 3D process were made in cylindrical geometry. It was found that the flow created a vortex in the water tank as planned, but resulted in disrupted fiber deposition. The rotation of the flow led to additional forces acting on the fibers, which were to be deposited on the core. As a result, fibers were partially torn from former deposition and the fiber bundles were separated too strongly, a situation that led to the formation of fiber agglomerates and spinnings as described by Hubbe et al. for the regular wet-laid nonwoven process [26]. To prevent this, pipe segments were inserted into the bottom plate of the wet-laid nonwoven tank. This allowed the direction of the water inflow to be adjusted. It was found that the formation of a vortex could be prevented when the water flow was directed directly towards the core. However, the same unfavorable formation of a vortex occurred again when the water inflow was in any way radially directed. Therefore, all further experiments were performed with the flow directed towards the core, which resulted in vortex prevention and thus homogenized the fiber deposition at the same time.

3.3. Manufacturing of the preforms

After a stable process was established, the C-fiber preforms were produced first. A total of three cylindrical preforms were manufactured to generate sufficient fiber material for the ceramic plate. The cylinders were cut open in axial direction while still wet and unrolled to obtain a 2D sheet. The masses of the nonwovens produced are summarized in Table 4. Secondly, the radome preform was produced with the same machine setup, but with the radome core. Despite the tight radius in the area of the tip, the preforms were obtained and displayed no defects (see Fig. 6). Two preforms were needed to achieve a sufficient fiber volume fraction. For this purpose, they were stacked into each other and processed as one preform during RTM. For the alumina fibers the same procedure was conducted and again three cylinders for the plate material were manufactured. For the radome two preforms were sufficient.

3.4. Ceramic manufacturing

After preform fabrication, these were converted into fiber-reinforced ceramics using LSI and PIP processes. Flat samples were made from the cylinder preforms and used for microstructure analysis and mechanical characterization. The radomes were prepared for wind tunnel testing

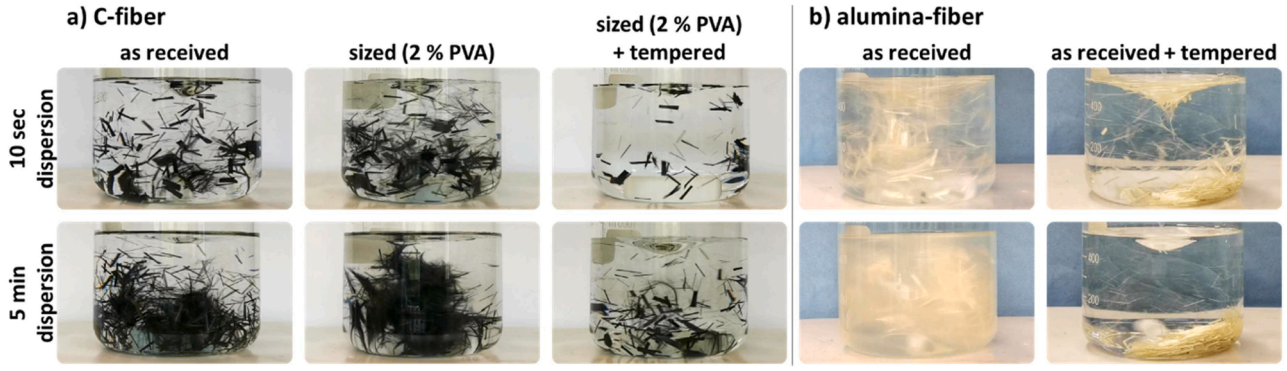

Fig. 5. Testing of fiber bundle dissolution for a) C- fibers as received, sized and sized + tempered, b) alumina-fibers *as received* and as received + tempered.

Table 4
Preform masses of the manufactured 3D preforms.

	Preform 1		Preform 2		Preform 3		∑ Preform
Preform	Mass (g)	Grammage (g/m^2)	Mass (g)	Grammage (g/m^2)	Mass (g)	Grammage (g/m^2)	FVF (%)
C-fiber / cylinder	49.2	984.0	28.0	560.0	29.2	584.0	40.1
C-fiber / radome	53.8	1349.8	40.1	1005.8			44.4
alumina-fiber / cylinder	94.0	1880.0	82.7	1654.0	114.8	2296.0	36.5
alumina-fiber / radome	113.2	2840.2	92.7	2324.6			43.1

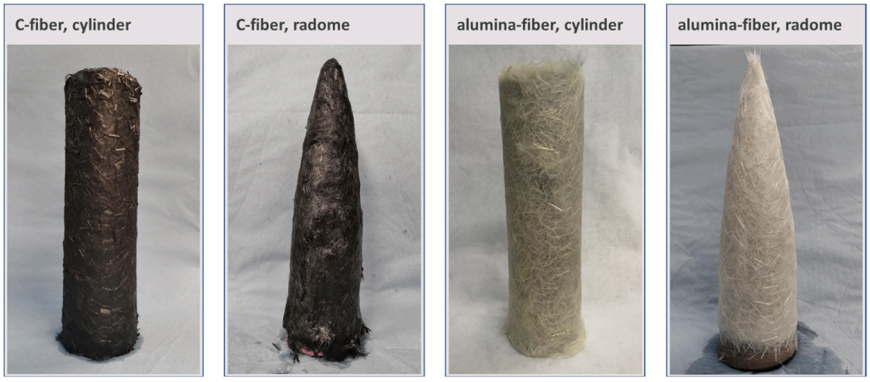

Fig. 6. 3D wet-laid nonwoven preforms manufactured in the laboratory 3D wet-laid nonwoven device.

and CT scanned before and after the tests. During the process, the porosity of the ceramic components was also measured using the Archimedes method. The results are summarized in Table 5, which also contains the bulk density in the final material condition. For the C/C-SiC samples, data acquisition was carried out to check whether process deviations were present. No such phenomena could be detected. For the OXIPOL samples, there was the additional function of determining, after how many PIP cycles a target porosity of less or equal 10% could be achieved. For the plate material, this was already achieved after a total of four cycles (9.47% open porosity). For the radome geometry, on the other hand, a total of six cycles were necessary, and yet the target porosity of less than 10% was not quite reached, but it was determined that the value was close enough to the set target (10.58% open porosity).

3.5. Characterization

The finished CMC samples were examined under a scanning electron microscope (SEM) with respect to their microstructure (Fig. 7). The microstructure shown corresponds to the expectations of wet-laid nonwoven reinforced C/C-SiC [13]. C/C blocks are formed which are surrounded by Si-SiC matrix. The block formation does not follow a regular pattern as it is known from fabric reinforcements, but is instead irregular. The investigation of the phase composition via the gray scale distribution showed 58.8% of carbon, 25.3% of SiC and 15.9% of unbound Si.

The OXIPOL samples show no gray scale contrast in SEM analysis. Therefore, no distinction between fiber and matrix in quantitative terms

Table 5
Open porosity of the C/C-SiC and OXIPOL samples during LSI and PIP process and density in the final material condition.

C/C-SiC	Infiltration	Pyrolysis	Siliconization					Density
plate	11.49%	24.20%	2.39%	-	-	-	-	2,06 g/cm^3
radome	7.05%	27.12%	3.17%	-	-	-	-	2,06 g/cm^3
OXIPOL	infiltration	pyrolysis 1	pyrolysis 2	pyrolysis 3	pyrolysis 4	pyrolysis 5	pyrolysis 6	
plate	10.11%	36.20%	25.91%	14.13%	9.47%	-	-	2,06 g/cm^3
radome	12.88%	39.41%	29.14%	23.30%	18.17%	13.62%	10.58%	2,06 g/cm^3

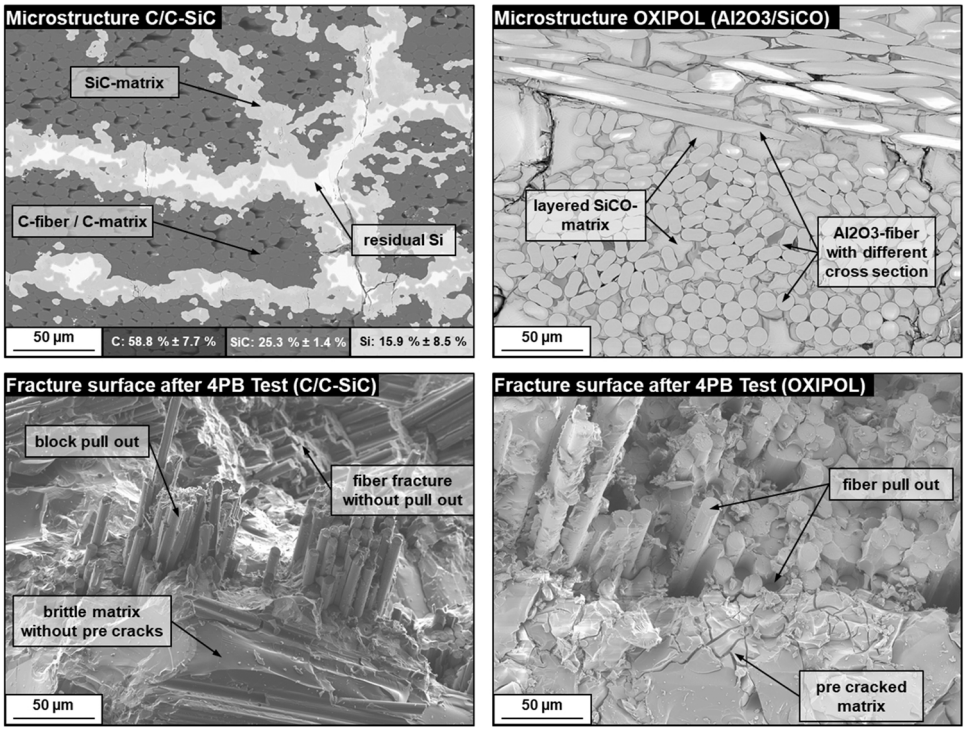

Fig. 7. Microstructure of the C/C-SiC and OXIPOL specimen on polished samples and fracture edges after the 4PB testing.

could be made with this method. The qualitative analysis of the fiber orientation results in an isotropic orientation. The microstructure of the matrix features dense blocks with partially no contact with the fibers due to shrinkage during pyrolysis. The post-infiltration cycles of the PIP process fill gaps in the matrix and improve the fiber matrix bonding. This layered structure of the matrix is visible in the images. In addition, the examination of the OXIPOL samples provided interesting insight regarding the filament cross sections of the Nextel 610 fibers. Different fiber cross sections could be detected, although the short fibers all came from the same ordering unit. It is known from studies by Pritzkow et al. that the fiber cross sections of Nextel 610 have a rather round cross section up to a filament count in roving of 4500, but above 10,000 filaments the cross section changes to a kidney shape [27]. Such mixed cross sections were observed in the short fibers used (Fig. 7). Accordingly, the short fibers appear to be a mixture of different roving thicknesses, which are converted to a uniform cut length. However, it is not possible to make any statements about the distribution of the roving parts used, and the effects of the different fiber cross sections on the ceramic have hardly been investigated so far.

After the 4PB tests, the microstructure at the fracture edges was examined. When analyzing the C/C-SiC samples, it was found that block pull out is observed wherever fibers lie parallel to the load direction (fibers lie parallel to the sample length) (Fig. 7). In areas where the fibers are deflected from the load direction, the fibers tend to break in a more brittle manner and apparently contribute less to the fracture toughness. In addition, the fracture edges show areas where predominantly matrix is present and thus brittle fracture can be observed. The OXIPOL wet laid nonwoven exhibits very similar fracture edge characteristics, but with the difference that increased fiber pull out is evident in the place of block pull out. Analogous to the C/C-SiC specimen, there are also partial areas with only a few fibers in which the matrix is dominant. Here, however, the matrix breaks more strongly along a large number of pre-cracks, which can be assigned to the individual matrix layers of the PIP process. This results in an increased amount of crack branching and thus crack energy dispersion even within the matrix-dominated areas.

The analysis of the strength has been carried out by means of 4-point-bending testing and is supplemented by the evaluation of the fracture toughness by means of the SENB test and the measurement of the interlaminar shear strength. The 4PB test shows that the flexural strength of the C/C-SiC material (67.66 ± 8.38 MPa on average) is higher than that of the short fiber OXIPOL (41.50 ± 5.66 MPa) (Fig. 8a and b). The same is true for elongation, with C/C-SiC (0.18 ± 0.05%) exceeding OXIPOL (0.10 ± 0.03%) almost twofold. Values of the study are summarized in Table 6. From the SENB test, the stress intensity factor K_I/displacement curves were received (Fig. 8c and d). Both materials show a stepped decrease in strength after reaching a maximum load, which can be attributed to crack deflection or crack stop when tearing further along the notch. In addition, the K_{Ic} value was determined (Table 6). It allows to compare both materials with each other in terms of their damage tolerance. For C/C-SiC a K_{Ic} of 2.03 MPa*$m^{1/2}$ and for OXIPOL of 3.55 MPa*$m^{1/2}$ was achieved, respectively. Accordingly, the results suggest that the OXIPOL material is more damage tolerant despite its lower strength. However, this needs to be further investigated in future research. The results of the shear compression test show that the C/C-SiC (14.50 MPa) material has a higher interlaminar shear strength than the OXIPOL (9.83 MPa) variant. This is mainly due to the SiC matrix reactively bonded with the carbon, which ensures a high cohesion of the nonwoven layers to each other. However, the inhomogeneity in the material results in a high standard deviation (4.19 MPa) and causes the material to lag behind measured values for fabric-reinforced C/C-SiC (24.8 MPa [28]). Due to the different matrix properties, the interlaminar shear strength of OXIPOL is low. The matrix cracks seen in Fig. 7 lead to rapid failure under predominant matrix loading and the very low percentage of fibers in the thickness direction.

Following the material analysis of the flat specimens, the radomes were prepared for the wind tunnel test. To detect irregularities or defects in the component, the C/C-SiC and the OXIPOL radome were CT scanned (Fig. 9). Both images show that the contours of the geometry could be mapped, but that there is significant inhomogeneity in the wall thickness. This is most extreme in the tip. Here, residues of the matrix are added to the material inhomogeneities. In the case of the C/C-SiC radome, areas with delaminations can be seen below the tip, which are presumably due to the two-layer structure of the preform. While the OXIPOL radome shows no delamination areas, the irregularity in the tip

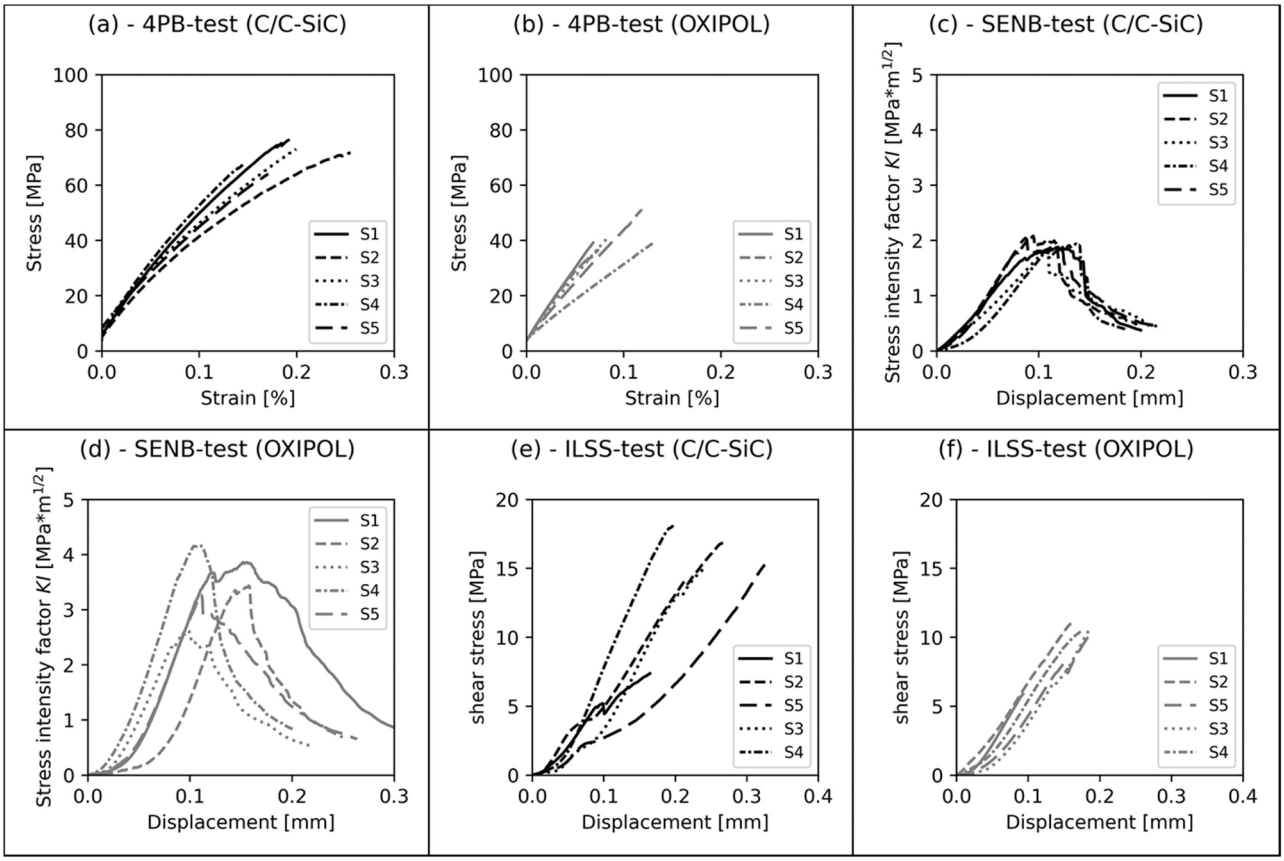

Fig. 8. Results of mechanical testing a), b) stress/strain curves of tested 4PB specimens, c), d) stress intensity factor K1/displacement curves of SENB samples, e), f) shear stress/displacement curves of ILSS test.

Table 6
Mechanical properties of C/C-SiC and OXIPOL.

	Stress [MPa]	Strain [%]	Young's modulus [GPa]	K_{Ic} [MPa*m$^{1/2}$]	ILSS [MPa]
C/C-SiC	67.66 ± 8.38	0.18 ± 0.05	44.33 ± 5.37	2.03 ± 0.21	14.50 ± 4.19
OXIPOL	41.50 ± 5.66	0.10 ± 0.03	42.35 ± 9.79	3.55 ± 0.56	9.83 ± 2.22

is extreme. In some areas, the wall thickness of the CMC is less than one millimeter. Despite these strong variations, it was decided to test both geometries in the wind tunnel setups to find out, in case of failure of the structures, where this is the case and therefore is the most critical.

3.6. Wind tunnel testing

The OXIPOL-radome successfully completed 18 test runs overall in both wind tunnels. First, in L2K, 12 tests at all three conditions and angles of attack up to ± 10° were conducted. In consecutive VMK testing, another 6 tests were done with angles of attack of ± 5° and roll angles of 0° and 90°. Exemplary results from infrared measurements of the surface temperature are shown in Fig. 10, and photographs of the radome before and after the tests are shown in Fig. 11.

As the images illustrate, the heating in L2K is much more concentrated on the nose region where very high temperatures of more than 1800 °C are reached for both low and high heat fluxes. In VMK, which produces an aerodynamically more representative flow, the heating of the radome is much more extensive to almost the entire surface. The pre-

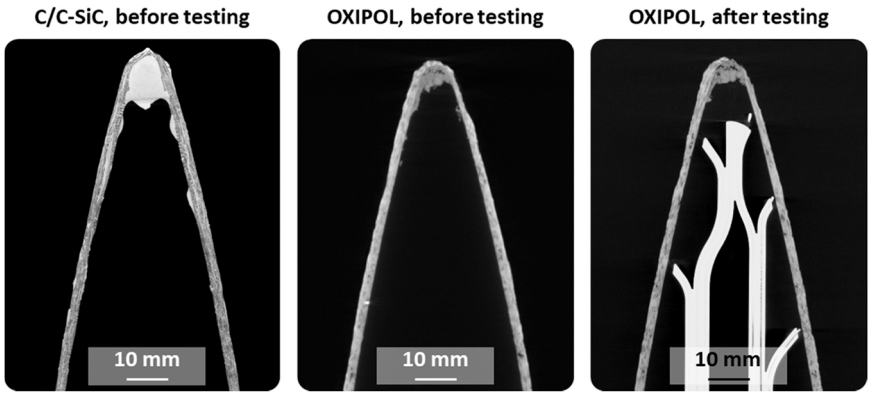

Fig. 9. CT scans of the radomes before and after testing.

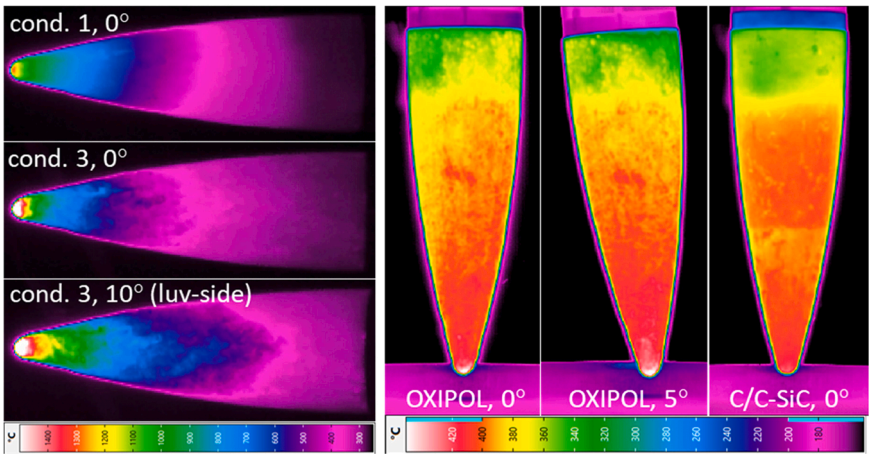

Fig. 10. Exemplary IR-images at end of test time in L2K (left side) and VMK (right).

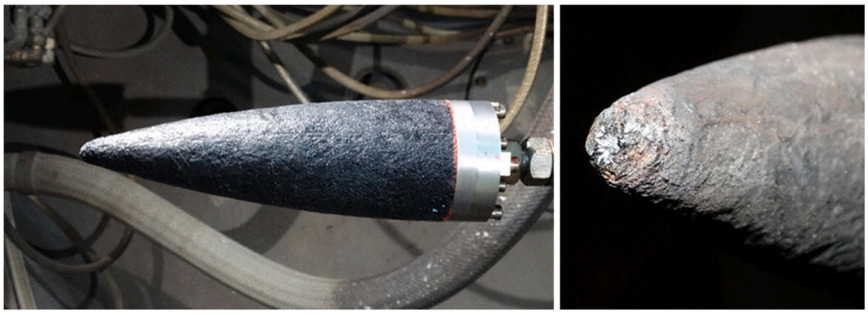

Fig. 11. OXIPOL radome before first (left) and after last (right) test in L2K.

and post-test photographs showed only very little recession of the radome nose tip. Also the VMK tests with much higher pressure and correspondingly high shear stress on the surface did not cause obvious removal of material.

For further post-test analysis, the radome was examined again in the CT (Fig. 9). Opposed to the appearance in Fig. 11, the images show that almost complete ablation has taken place in the tip area, especially where the wall thickness before testing was only one millimeter. At this point, the tip is almost only closed by matrix deposited on the inside. Apart from the tip, no other areas with material removal could be detected. This demonstrates both the strength and durability of the material as despite the extent of ablation, a critical component failure was prevented although the radome had been subjected multiple times to the loads expected in its real application. On the other hand, it also illustrates that improvements in radome manufacture are imperative, particularly in this critical area.

The C/C-SiC radome was first tested in VMK and tests in L2K were only planned afterwards, simply for timely reasons. However, this turned out to be very unfortunate, as the radome was destroyed during the first wind tunnel test in VMK. After it had successfully passed the nominal test duration including data acquisition (Fig. 10), the radome surprisingly detached from the mount during the shutdown of the test rig. Despite the structure still being subjected to a near Mach 3 flow with a total pressure of around 17 bar and still being placed completely inside the Mach rhombus of the flow, the radome moved about 10 mm against the flow direction before it was pushed back against the model holder and broke as illustrated in Fig. 12. Supplementary investigations showed an increase of the internal pressure in the C/C-SiC radome. An analysis with the aid of CFD computations indicates that it might be possible that the force induced by this internal pressure exceeds the aerodynamical force of the oncoming flow. This force, in combination with an imperfect test setup (glue not properly hardened/dried) could have caused the

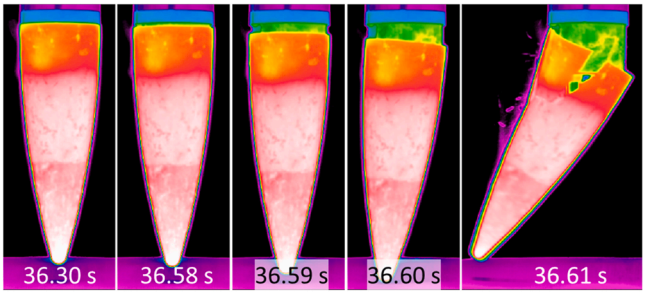

Fig. 12. IR-images of destruction of C/C-SiC radome during wind tunnel shut down.

failure of the glue connection of the radome to the model holder and thus the radome to be destroyed. It should be noted that there is no clear evidence to support this theory but given the circumstances, it seems to be the most likely explanation.

4. Discussion

Based on the results, the following insights into the potential of the 3d wet-laid nonwoven process were gained. Two elementary requirements were developed for the 3D wet-laid process: First, the sizing of the fiber bundles to keep them stable in the process and, second, the flow control in the suspension vessel of the wet-laid nonwoven line. The first was achieved by stabilizing the bundle structure with a PVA sizing and its thermal post-crosslinking. For the flow guidance, the original configuration was modified with a tangentially directed inflow into the vessel. The empirical investigation of different inflow angles showed that the direct inflow into the core, i.e. into the center of the container, is

best suited for vortex free flow. As a result, fiber spinning does not occur and the fiber bundles are deposited on the core as designed. Carbon and alumina preforms were produced using this process. Fiber deposition was successful on both, but differences can be seen in the area of the tip (Fig. 6). The carbon fibers were deposited well on the tip (tip radius 3 mm). The alumina fibers, on the other hand, do not follow the outline accurately, since they cannot bend according to the curvature due to their high stiffness. In addition to the degree of crystallization, the decisive factor for the high stiffness of the fibers is the fiber diameter [29]. This is significantly higher for alumina fibers than for carbon fibers (alumina approx. 14 μm, carbon 6 μm). At such high stiffness, fibers can only be laid down following the contour if the fiber length is shorter than the smallest radius of the geometry. This effect increases significantly the more the bundle structure is retained, since this "increased" fiber diameter also increases the stiffness. In order to achieve tight component curvatures with undissolved fiber bundles in the wet-laid nonwoven process, the fibers should be significantly shorter than the smallest diameter, to achieve the best preform results.

The shaping of the CMC production then took place via RTM. While flat specimens were produced from the cylinders, the radomes were manufactured according to the preform geometry. Here, the structure of the RTM molds in particular had a strong influence on the quality of the tip. Fig. 9 shows strong irregularities of the wall thickness in the tip. These cannot be attributed to the preform. The defects in the tip are due to the current RTM setup, there preforms are slipped onto the core and then pushed together into the negative form. However, since a large part of the radome mold has an almost cylindrical structure, the preforms are partially trapped between the core and the outer wall when they are pushed in. As a result, when pushed further, the tip is partially pierced and the fiber material is not transported all the way into the tip. In particular, since the nonwovens have low strength, they tear quickly and puncturing becomes more likely. Here, a more suitable setup for molding needs to be found in the future to accommodate the more fragile nonwovens compared to, for example, fabric preforms. However, all the wet-laid nonwoven preforms could successfully be processed via LSI or PIP process to fiber reinforced ceramics, which highlights the possibilities of the new preforming method.

In addition, it was not only possible to demonstrate the manufacturing possibilities, but also to investigate the materials and carry out initial application studies. While the results of the microstructure investigation show a satisfactory material composition, the mechanical investigations and the evaluation of the fracture toughness showed that the existing material still needs to improve significantly in terms of strength and fracture toughness. One reason for this is that the load-bearing properties of a CMC material are dramatically reduced when fibers are not oriented in the load direction [29,30]. Assuming that within wet-laid nonwovens there is an almost isotropic fiber orientation in the X/Y plane of the nonwoven, only a small proportion of these are oriented in the load direction. One approach to improve these properties could be to increase the fiber volume content (currently approx. 40%), since this would also increase the fibers oriented in the load direction across the material. This approach should be further investigated to increase the mechanical properties of the materials in the future.

The wind tunnel tests have shown that load-bearing components can also be produced with the current preform and process setup. The durability and protection of the internal hardware can be made possible with both material variants. While the OXIPOL radome performed well and withstood a total of 18 tests, the C/C-SiC radome was destroyed during the first VMK run. As described before the radome detached itself from the sample holder of the wind tunnel during shut down phase of the first run due to insufficient hardened glue. Despite the remaining aerodynamical force of the oncoming flow it was pushed of the holder and after the complete detachment accelerated against the holder and therefore destroyed. The supplementary measurement of the inner pressure suggests, that the higher pressure inside the radome could have further supported the detachment. One factor that might have contributed to the pressure build up could be the low porosity of the C/C-SiC material (3.17%) as compared to other CMC radomes previously studied (10–20%). Thus, it has a significantly less potential for outgassing in the event of possible gas developments or internal pressure build-up. This is an aspect that has to be investigated more closely and needs to be carefully considered in future experimental setups or the actual use of the material for the designated application. In addition, it has to be considered that when using C/C-SiC, the application of an Environmental Barrier Coating (EBC) would also be beneficial to prevent oxidation effects, which could also lead to failure. Depending on the application scenario and the resulting maximum flight time, it must be decided whether it is necessary to provide the radome with this coating. When using C/C-SiC, however, at least the additional integration of a radar-transparent window is necessary, in contrast to OXIPOL, which is radar-transparent as an overall component. However, it is important to emphasize at this point that it was not the material that led to the failure of the component, but the connection to the test rig in the form of the adhesive. Nevertheless, due to the loss of the C/C-SiC-sample during test, future test campaigns have to shine light on the material's performance regarding, abrasion, oxidation, and material removal, as happened with the OXIPOL radome.

5. Conclusion

The aim of the work was to find a suitable preform method with which complex component shapes can be produced beyond flat samples. Wet-laid nonwoven technology was identified as a potentially interesting technique and a laboratory process was set up with which 3D preforms can be implemented. The target geometry of this study was radomes, since these cover problem areas well (small radius tip) and there was the possibility of subjecting the CMC component to an application-oriented test.

The developed preforming process opens up new possibilities for component manufacture in all areas of application in which more complex geometries have to be realized and no cost-effective preform manufacture was previously possible. The manufacturing was explored and suitable process settings were determined. For the low mechanical strength of the wet-laid nonwoven the RTM green body manufacturing needs to be adapted, to prevent the tearing of the textile. However, further studys need to target an increase in strength of the material by higher the FVF. Specific to the radome the wet-laid nonwoven OXIPOL material has performed well and is of great interest for this application.

Over all, the 3D wet-laid nonwoven technology was found to be promising for CMC manufacturing and can make an important contribution to the further commercialization of CMCs, due to its low production costs and flexibility in component geometry.

CRediT authorship contribution statement

F.K. designed, conducted, and analyzed experiments and wrote the manuscript. M.F. and O.H. designed and conducted experiments and edited the manuscript. All remaining authors were involved in data analysis and edited the manuscript.

Declaration of Competing Interest

The authors declare the following financial interests/personal relationships which may be considered as potential competing interests: Patent EP3980388A1 'Method for producing a near-net-shape fiber body, fiber body, method for producing a ceramic component, and ceramic component'. Inventors: Fiona Kessel, Linda Klopsch, Martin Frieß, Charlotte Zöllner. Assignee: German Aerospace Center.

Data Availability

Data will be made available on request.

Acknowledgments

This research is funded by the German Ministry of Defence (BMVg) and part of the DLR project 'ITEM-FK' and 'FK2020+'. The authors would like to sincerely thank, Daniel Cepli, Stefan Frick, Marco Alexander Smolej, Elena Carcano and Alice Thomas at the DLR-Institute of Structures and Design for their technical support. Sincere thanks go to Prof. Dietmar Koch from Augsburg University for his support in data analysis.

References

[1] A. Mountasir, M. Löser, G. Hoffmann, C. Cherif, K. Großmann, 3D Woven Near-Net-Shape Preforms for Composite Structures, Adv. Eng. Mater. vol. 18 (2016) 391–396.
[2] C. Weimer, T. Preller, P. Mitschang, K. Drechsler, Approach to net-shape preforming using textile technologies. Part II: holes, Compos. Part A: Appl. Sci. Manuf. vol. 31 (2000) 1269–1277.
[3] C. Weimer, T. Preller, P. Mitschang, K. Drechsler, Approach to net-shape preforming using textile technologies. Part I: edges, Compos. Part A: Appl. Sci. Manuf. vol. 31 (2000) 1261–1268.
[4] J. Rybicka, A. Tiwari, G. Leeke, Technology readiness level assessment of composites recycling technologies, J. Clean. Prod. vol. 112 (2016) 1001.
[5] F. Süß, T. Schneider, M. Frieß, R. Jemmali, F. Vogel, L. Klopsch, et al., Combination of PIP and LSI processes for SiC/SiC ceramic matrix composites, Open Ceram. vol. 5 (2021), 100056.
[6] O. Hohn, B. Esser, J. Klevanski, A. Gülhan, R. Fener, B. Panthen, et al., Experimental investigations for the thermal qualification of high speed missile radomes, 8th Eur. Conf. Aeronaut. Space Sci. (EUCASS) (2019).
[7] F. Breede, S. Hofmann, N. Jain, R. Jemmali, Design, manufacture, and characterization of a carbon fiber-reinforced silicon carbide nozzle extension, Int. J. Appl. Ceram. Technol. vol. 13 (2016) 3–16.
[8] M. Frieß and S. Denis, "Oxide CMC Components Manufactured via PIP Processing Based on Polysiloxanes," presented at the ECerS XII, Stockholm, Schweden, 2011.
[9] J. Nie, Y. Xu, L. Zhang, L. Cheng, J. Ma, Microstructure and tensile behavior of multiply needled C/SiC composite fabricated by chemical vapor infiltration, J. Mater. Process. Technol. vol. 209 (2009) 572–576.
[10] X. Chen, L. Chen, C. Zhang, L. Song, D. Zhang, Three-dimensional needle-punching for composites – a review, Compos. Part A: Appl. Sci. Manuf. vol. 85 (2016) 12–30.
[11] G. Batch, S. Cumiskey, C. Macosko, Compaction of fiber reinforcements, Polym. Compos. vol. 23 (2002) 307–318.
[12] W. Albrecht, H. Erth, H. Fuchs, Vliesstoffe: Rohstoffe, Herstellung, Anwendung, Eigenschaften, Prüfung, Wiley, 2012.
[13] F. Kessel, L. Klopsch, V. Jehle, N.-J. Biller, M. Frieß, Y. Shi, et al., Wet-laid nonwoven based ceramic matrix composites: An innovative and highly adaptable short fiber reinforcement for ceramic hybrid and gradient materials, J. Eur. Ceram. Soc. vol. 41 (2021) 4048–4057.
[14] R. Wever, D. Twede, The history of molded fiber packaging: a 20th century pulp story, Proc. 23rd IAPRI Symp. . Packag., Windsor, UK September 3–5 (2007).
[15] M. Onilude, T. Omoniyi, B. Akinyemi, K. Adigun, The design and fabrication of a recycled paper egg tray machine, Int. J. Contemp. Manag. vol. Vol. 3 (2012) 142–151.
[16] F. Khalid, M. Tabish, K. Bora, Novel poly(vinyl alcohol) nanofiltration membrane modified with dopamine coated anatase TiO2 core shell nanoparticles, J. Water Process Eng. vol. 37 (2020), 101486.
[17] B.H. Musa, N.J. Hameed, Study of the mechanical properties of polyvinyl alcohol/starch blends, Mater. Today.: Proc. vol. 20 (2020) 439–442.
[18] K.K.H. Wong, M. Zinke-Allmang, W. Wan, Effect of annealing on aqueous stability and elastic modulus of electrospun poly(vinyl alcohol) fibers, J. Mater. Sci. vol. 45 (2010) 2456–2465.
[19] R. Kochendörfer, Liquid Silicon Infiltration- A Fast and Low Cost CMC-Manufacturing Process, 1991.
[20] F.H. Gern, R. Kochendörfer, Liquid silicon infiltration: description of infiltration dynamics and silicon carbide formation, Compos. Part A: Appl. Sci. Manuf. vol. 28 (1997) 355–364.
[21] B. Mainzer, M. Frieß, R. Jemmali, D. Koch, Development of polyvinylsilazane-derived ceramic matrix composites based on Tyranno SA3 fibers, J. Ceram. Soc. Jpn. vol. 124 (2016) 1035–1041.
[22] M. Kuntz, J. Horvath, G. Grathwohl, High temperature fracture toughness of a C/SiC (CVI) composite as used for screw joints in re-entry vehicles, High. Temp. Ceram. Matrix Compos. (2001) 469–473.
[23] E.-O.K. Klaus Triesch, The vertical test section (VMK) at DLR in Cologne-Porz vol. Technical Translation of DFVLR-Mitt-86–22. Germany: European Space Agency, 1986.
[24] A. Gülhan, B. Esser, Arc-heated facilities as a tool to study aerothermodynamic problems of reentry vehicles, Prog. Astronaut. Aeronaut. vol. 198 (2002) 375–403.
[25] A. Gülhan B. Esser U. Koch K. Hannemann Mars entry simulation in the arc heated facility L2K L2K 2002.
[26] M. Hubbe, A. Koukoulas, Wet-laid nonwovens manufacture – chemical approaches using synthetic and cellulosic fibers, BioResources vol. 11 (2016) 5500–5552.
[27] W.E.C. Pritzkow, R.S.M. Almeida, L.B. Mateus, K. Tushtev, K. Rezwan, All-oxide ceramic matrix composites (OCMC) based on low cost 3M Nextel™ 610 fabrics, J. Eur. Ceram. Soc. vol. 41 (2021) 3177–3187.
[28] Y. Shi, F. Kessel, M. Frieß, N. Jain, K. Tushtev, Characterization and modeling of tensile properties of continuous fiber reinforced C/C-SiC composite at high temperatures, J. Eur. Ceram. Soc. vol. 41 (2020), 10/02.
[29] Y. Shi, "Characterization and modeling of the mechanical properties of wound oxide ceramic composites," 2017, 2017.
[30] M. Cordin, T. Bechtold, T. Pham, Effect of fibre orientation on the mechanical properties of polypropylene–lyocell composites, Cellulose vol. 25 (2018) 7197–7210.